Lattice EFG tensors at the rare-earth metal sites in $RBa_2Cu_3O_7$ and $La_{2-x}Sr_xCuO_4$

1995 J. Phys.: Condens. Matter 7 2345

(http://iopscience.iop.org/0953-8984/7/11/013)

J. Phys.: Condens. Matter 7 (1995) 2345–2352. Printed in the UK

Lattice EFG tensors at the rare-earth metal sites in $RBa_2Cu_3O_7$ and $La_{2-x}Sr_xCuO_4$

V F Masterov, F S Nasredinov, N P Seregin, P P Seregin and M A Sagatov
St Petersburg State Technical University, 195251, St Petersburg, Russia

Received 30 September 1994

Abstract. Parameters of the tensors of the electric field gradient (EFG) created by lattice ions at the rare-earth metal (REM) sites in $RBa_2Cu_3O_7$ (R is a REM or Y) and $La_{2-x}Sr_xCuO_4$ ($0 < x < 0.3$) have been determined by means of $^{155}Eu(^{155}Gd)$ emission Mössbauer spectroscopy. The EFG tensors at the REM sites have been calculated in the point charge approximation. The experimental and calculated EFGs are shown to be in good agreement when holes are supposed to be mainly in sublattices of the chain and Cu–O plane oxygen for $RBa_2Cu_3O_7$ and $La_{2-x}Sr_xCuO_4$, respectively.

1. Introduction

The spatial distribution of charges among sites in ionic lattices can be determined by comparing the experimental and calculated parameters of the electric field gradient (EFG) tensors. Generally, the U_{pp} components of a diagonalized EFG tensor at a nucleus consist of two parts

$$U_{pp} = (1 - \gamma)V_{pp} + (1 - R_0)W_{pp} \tag{1}$$

where V_{pp} and W_{pp} are tensor components of the EFG created by lattice ions (lattice EFG) and by valence electrons related to the nucleus (valence EFG), respectively; γ and R_0 are the Sternheimer factors, p is the Cartesian coordinate.

The lattice EFG may be calculated using the point charge model [1], whereas the valence EFG is given by various quantum-mechanical methods [2, 3]. The validity of the results of the latter might evoke some doubt, and, therefore, probe atoms with spherical electron shells, i.e., without valence contribution to equation (1), are preferable for measuring EFG. For this reason we have proposed emission Mössbauer spectroscopy with the $^{67}Cu(^{67}Zn)$ isotope as a method for experimental determination of the EFG tensor in copper-based HTSCs. In this technique a Zn^{2+} ion with a spherical $3d^{10}$ electron shell, and, consequently, without valence EFG, appears at a copper site after the decay of the parent ^{67}Cu nucleus [4].

The above technique allowed us to find the effective charges of oxygen ions for $YBa_2Cu_3O_7$ [5] and $La_{2-x}Sr_xCuO_4$ [6], with certain assumptions made regarding the cation charges. Agreement between the calculated and experimental parameters of the lattice EFG tensors for $YBa_2Cu_3O_7$ may be achieved by using two kinds of model. Both imply the presence of a hole in the immediate vicinity of the chain copper, either at the chain oxygen (model A) or at the bridging (apical) oxygen (model B). Additional evidence is necessary for one of these to be chosen. A similar procedure carried out for $La_{2-x}Sr_xCuO_4$ has shown that holes mainly reside at the oxygen sites lying in the Cu–O planes [6], though in this case,

0953-8984/95/112345+08$19.50

too, additional evidence is desirable. The present work proposes ^{155}Eu(^{155}Gd) emission Mössbauer spectroscopy as a source of the necessary additional evidence for $RBa_2Cu_3O_7$ compounds (R is a rare-earth metal (REM) or Y) and for the $La_{2-x}Sr_xCuO_4$ solid solutions with $0.1 < x < 0.3$.

2. Experimental details

The principle of the technique used consists in extraction of a carrier-free preparation of the ^{155}Eu parent activity, followed by synthesis of ^{155}Eu-doped ceramic samples and by recording of their ^{155}Eu(^{155}Gd) emission Mössbauer spectra. ^{155}Eu has been considered to occupy the REM sites in the above substances, which is supported by the chemical similarity of all rare-earth metals. Therefore, the ^{155}Gd Mössbauer probe produced after the decay of ^{155}Eu should also reside at a regular REM site. The carrier-free ^{155}Eu preparation allows for low Mössbauer impurity concentrations and enables one to use structural data for undoped $RBa_2Cu_3O_7$ and $La_{2-x}Sr_xCuO_4$ when analysing the results.

Typical for the Gd^{3+} ion is the $^6S_{7/2}$ state with a half-filled spherical $4f^7$ shell. For this reason the EFG at ^{155}Gd nuclei is expected to be created only by lattice ions.

The ^{155}Eu activity was produced by the ^{154}Sm(n, γ)^{155}Sm reaction followed by β decay of ^{155}Sm. The carrier-free ^{155}Eu preparation was then separated chromatographically, since the half-lives of ^{155}Eu and the intermediate nucleus ^{155}Sm are 4.96 years and 23 min, respectively. The separation was carried out in six months after the reactor irradiation for the decay of the residual activity of ^{156}Eu with a half-life of 15 d.

Ceramic samples of $RBa_2Cu_3O_7$ (R is Nd, Sm, Eu, Gd, Dy, Y or Tm) and $La_{2-x}Sr_xCuO_4$ were prepared by sintering the corresponding oxides. The ^{155}Eu activity was added to the starting mixture. Test samples of $RBa_2Cu_3O_7$ had an orthorhombic structure and critical temperatures T_c of about 85 K. Test samples of $La_{2-x}Sr_xCuO_4$ had a tetragonal structure and T_c values of 26, 40, 35 and < 5 K for $x = 0.1$, 0.15, 0.2 and 0.3, respectively.

The Mössbauer spectra (86.5 keV transition) were recorded at 80 K using a singlet $GdPd_3$ absorber. The 86.5 keV radiation was detected by a NaI(Tl) detector with a Pb critical filter that suppressed the 60 keV and 105 keV radiation of ^{155}Eu and the rest of the 89 keV radiation of ^{156}Eu. For this reason the ^{155}Gd 86.5 keV spectra were recorded predominantly. The ^{155}Gd 105 keV spectra were additionally suppressed due to the high measuring temperature. The ^{155}Gd 60 keV spectra were not observed in the velocity range used because of their large line width of about 30 mm s^{-1}.

Typical spectra are shown in figures 1 and 2. The results of the processing of these are listed in table 1.

3. Experimental results and discussion

3.1. $RBa_2Cu_3O_7$ compounds

The emission Mössbauer spectra of the $RBa_2Cu_3O_7$: ^{155}Eu samples are quadrupole doublets, which points to a non-cubic environment of the REM sites. The isomer shifts of all spectra correspond to Gd^{3+}. It is important that the quadrupole splitting S increases with increasing radius r of the REM ion (see figure 3(a)). The quadrupole splitting of the ^{155}Gd Mössbauer spectra is determined by the ground state of the nucleus (spin $I = \frac{3}{2}$, quadrupole moment $Q = 1.59$ b) and is described as follows

$$S = \tfrac{1}{2}|eQU_{zz}|\left(1 + \frac{n^2}{3}\right)^{1/2} \tag{2}$$

Table 1. Parameters of $^{155}Eu(^{155}Gd)$ emission Mössbauer spectra of $RBa_2Cu_3O_7$ and $La_{2-x}Sr_xCuO_4$ ceramics.

Composition	IS[a] (mm s^{-1})	S[b] (mm s^{-1})
$NdBa_2Cu_3O_7$	−0.50	1.70
$SmBa_2Cu_3O_7$	−0.52	1.61
$EuBa_2Cu_3O_7$	−0.51	1.48
$GdBa_2Cu_3O_7$	−0.52	1.43
$DyBa_2Cu_3O_7$	−0.51	1.19
$YBa_2Cu_3O_7$	−0.51	1.19
$TmBa_2Cu_3O_7$	−0.50	1.00
$La_{1.9}Sr_{0.1}CuO_4$	−0.50	1.43
$La_{1.85}Sr_{0.15}CuO_4$	−0.52	1.41
$La_{1.8}Sr_{0.2}CuO_4$	−0.52	1.39
$La_{1.7}Sr_{0.3}CuO_4$	−0.51	1.36
	±0.02	±0.02

[a] IS is the isomer shift relative to $GdPd_3$.
[b] S is the quadrupole splitting.

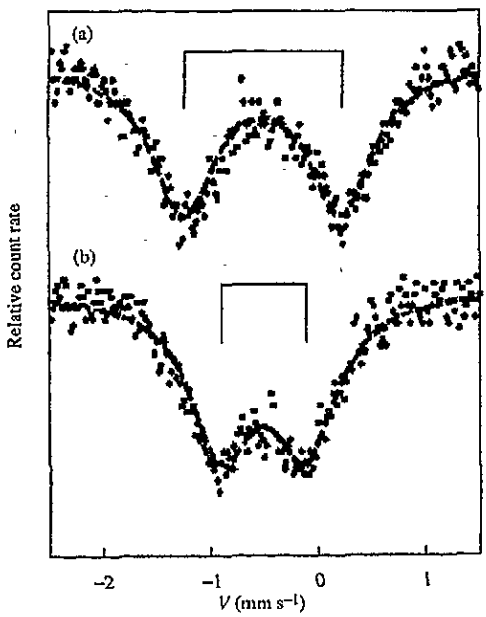

Figure 1. $^{155}Eu(^{155}Gd)$ emission Mössbauer spectra of (*a*) $NdBa_2Cu_3O_7$ and (*b*) $TmBa_2Cu_3O_7$.

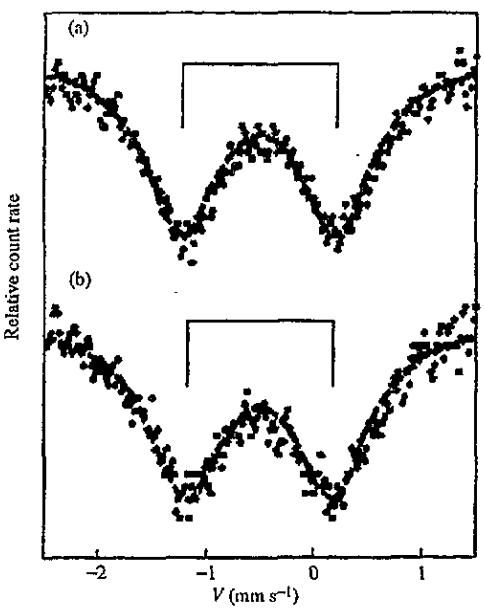

Figure 2. $^{155}Eu(^{155}Gd)$ emission Mössbauer spectra of (*a*) $La_{1.9}Sr_{0.1}CuO_4$ and (*b*) $La_{1.7}Sr_{0.3}CuO_4$.

where U_{zz} is the principal component of the total EFG tensor at the ^{155}Gd nucleus; $n = (U_{xx} - U_{yy})/U_{zz}$ is the asymmetry parameter of the total EFG tensor. For the tensor components the inequality $|U_{xx}| < |U_{yy}| < |U_{zz}|$ should be valid.

Thus, the value of S is proportional to U_{zz}, which is determined by the lattice EFG for the Gd^{3+} probe

$$U_{zz} = (1 - \gamma)V_{zz} \tag{3}$$

where V_{zz} and γ relate to the REM sites and Gd^{3+} ion, respectively.

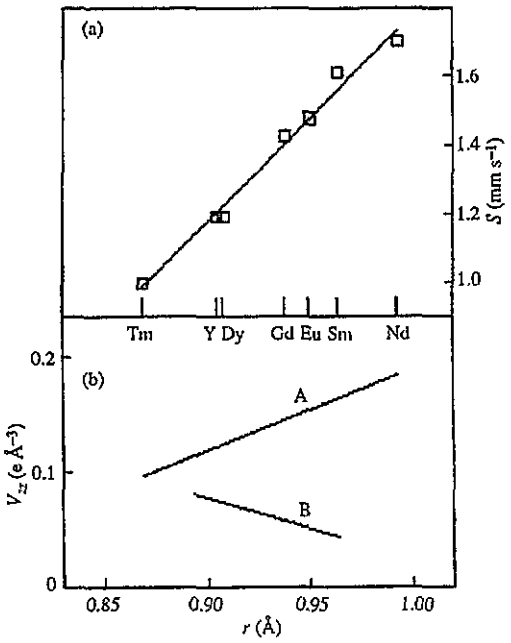

Figure 3. (*a*) Dependence of the quadrupole splitting S of the $RBa_2Cu_3O_7$:^{155}Eu Mössbauer spectra on the rare-earth ion radius r. (*b*) Dependences of the calculated principal components V_{zz} of the lattice EFG tensors at the REM sites of the $RBa_2Cu_3O_7$ compounds on r for models A and B. $V_{zz} < 0$ in both cases, but $|V_{zz}|$ is plotted for comparison with figure 3(*a*).

We have calculated the lattice EFG tensor components V_{pp} for all sites of the $RBa_2Cu_3O_7$ lattices in the point charge approximation (see detailed information in [7]). The lattice was considered as a superposition of eight sublattices according to the structural formula $RBa_2Cu(1)Cu(2)_2O(1)_2O(2)_2O(3)_2O(4)$. Since various versions of oxygen site numbering are accepted in the literature, our designations are shown in figure 4. The structural parameters used in calculating the lattice EFG for the $RBa_2Cu_3O_7$ compounds were taken from [8, 9]. All the calculated EFG tensors proved to be diagonal in the crystal axes.

Table 2. Effective atomic charges in the $YBa_2Cu_3O_7$ lattice. The charges have been determined as described in [7], with the experimental data related to the Cu(1), Cu(2), O(1), O(2) and Cu(1), Cu(2), O(2), O(4) sites for models A and B, respectively.

Y	Ba	Cu(1)	Cu(2)	O(1)	O(2)	O(3)	O(4)	Model
+3	+2.05	+2.13	+2.16	−2.17	−2.01	−1.90	−1.38	A
+3	+3.28	+1.23	+1.31	−1.44	−1.96	−1.85	−2.91	B

Previously [7] we used the results of the lattice EFG calculations for the Cu(1), Cu(2), O(1), O(2) and O(4) sites in $YBa_2Cu_3O_7$ as well as the parameters of the quadrupole coupling tensors for ^{67}Zn at the copper sites [4] and for ^{17}O at the oxygen sites [10] to determine the charge distribution among the sites for both models A and B (see table 2). Then the lattice EFG tensors were calculated at the REM sites using both charge distributions. Figure 3(*b*) shows the slopes of the calculated $V_{zz}(r)$ dependences having opposite signs

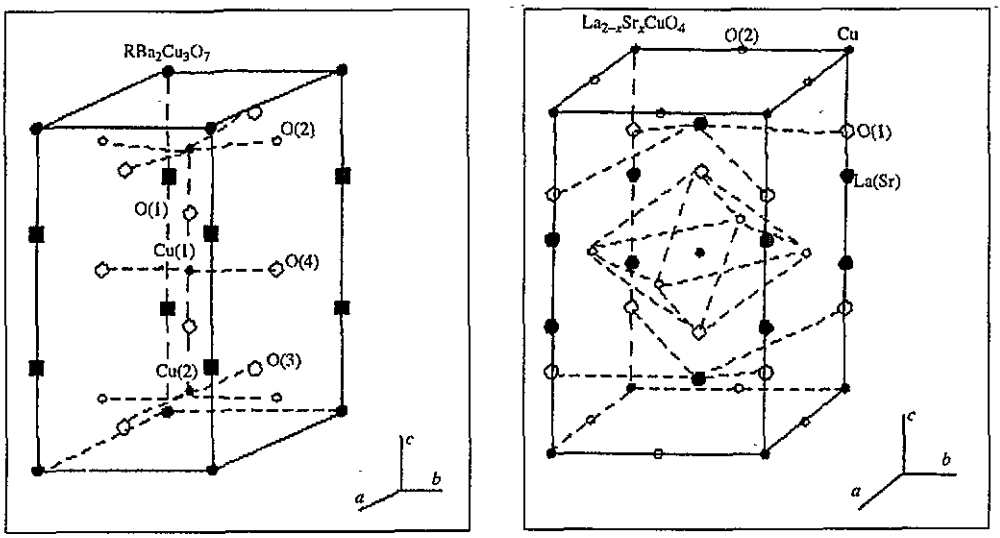

Figure 4. The unit cells of $RBa_2Cu_3O_{7-x}$ and $La_{2-x}Sr_xCuO_4$.

for models A and B. The z-axes of the calculated EFG tensors are also different for different models. The z-axis coincides with the crystal axes c and a for models A and B, respectively. Unfortunately, our $^{155}Eu(^{155}Gd)$ data for ceramic samples are insensitive to the direction of the z-axis. A qualitative agreement between the measured $S(r)$ dependence (figure 3(a)) and the calculated $V_{zz}(r)$ one (figure 3(b)) is found only for model A. Thus, the $^{155}Eu(^{155}Gd)$ emission Mössbauer data support model A for the $RBa_2Cu_3O_7$ compounds.

However, this conclusion is valid only if the EFG at the Gd^{3+} probe nuclei is created solely by the lattice ions. To examine this condition we have plotted the dependence of S on $s = V_{zz}(1 + n_{latt}^2/3)^{1/2}$, where n_{latt} is the asymmetry parameter defined similarly to n in equation (2). Figure 5 shows that this dependence for model A is satisfactorily described by a straight line. An extrapolation of the latter to $s = 0$ gives the value $S_0 = -(0.10 \pm 0.08)$ mm s^{-1}, which is small compared with the experimental values of S. Therefore, the dependence in figure 5 could be considered as an approximately direct proportionality.

The quadrupole splitting of the ^{155}Gd Mössbauer spectra is described by the following equation derived from equations (1) and (2)

$$S = \tfrac{1}{2}|eQ||(1-\gamma)V_{zz} + (1-R_0)W_{zz}|\left(1+\frac{n^2}{3}\right)^{1/2} \tag{4}$$

where

$$n = \frac{(1-\gamma)V_{zz}n_{latt} + (1-R_0)W_{zz}n_{val}}{(1-\gamma)V_{zz} + (1-R_0)W_{zz}}.$$

Here, γ and R_0 are the Sternheimer factors for Gd^{3+}, n_{val} is the asymmetry parameter of the valence EFG tensor.

It can be seen from equation (4) that the direct proportionality in figure 5 evidences a small valence EFG at the ^{155}Gd nuclei.

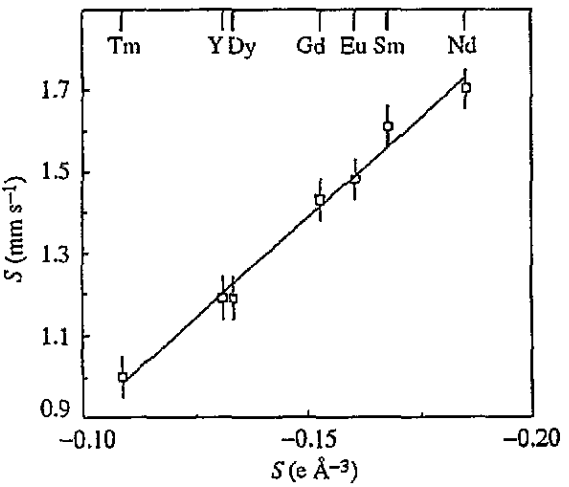

Figure 5. Dependence of the quadrupole splitting S of the $RBa_2Cu_3O_7$:^{155}Eu Mössbauer spectra on the parameters of the calculated lattice EFG tensor at the REM sites.

The valence contribution $(1 - R_0)W_{zz} > 0$, since $V_{zz} < 0$ and $S_0 < 0$. Its magnitude can be estimated by the quantity $|S_0/eQ| = 0.13 \pm 0.10$ e Å^{-3}. The slope of the straight line in figure 5 corresponds to the Sternheimer factor for the Gd^{3+} ion $\gamma = -(24.2 \pm 2.0)$, which gives the values of the lattice contribution $(1 - \gamma)V_{zz}$ in the range from -2.45 to -4.60 e Å^{-3} for the $RBa_2Cu_3O_7$ compounds investigated. It should be noted that the above value $\gamma = -24.2$ is only a rough estimation. For instance, it is considerably less than the value $\gamma = -60.87$ resulting from quantum-mechanical calculations [11].

3.2. *$La_{2-x}Sr_xCuO_4$ solid solutions*

The results of section 3.1 show that ^{155}Eu(^{155}Gd) Mössbauer spectroscopy is applicable for determining the lattice EFG at the REM sites. In this connection we have carried out ^{155}Eu(^{155}Gd) Mössbauer investigations of $La_{2-x}Sr_xCuO_4$ solid solutions. The corresponding spectra are shown in figure 2 and their parameters are listed in table 1. The isomer shifts observed for all the spectra indicate that Gd is in the Gd^{3+} state, and the quadrupole splitting decreases with x increasing from 0.1 to 0.3.

We calculated the lattice EFG tensor parameters V_{zz} and n_{latt} at La sites of the $La_{2-x}Sr_xCuO_4$ lattice which was considered as a superposition of four sublattices $(La, Sr)_2CuO(1)_2O(2)_2$ (figure 4). The atomic positions in the unit cell and the dependence of the lattice parameters on x were taken from [12] and [13], respectively.

Due to ambiguity in the Sternheimer factor we found it impossible to compare directly the experimental values of S with the calculated ones given by

$$S = -\tfrac{1}{2}|eQV_{zz}|\left(1 + \frac{n_{latt}^2}{3}\right)^{1/2}(1 - \gamma). \tag{5}$$

For this reason we compared the ratios $P = S_x/S_{x=0.1}$ of the experimental and calculated $p = s_x/s_{x=0.1}$ values, as had been done earlier for similar ^{67}Cu(^{67}Zn) Mössbauer data [6]. Here the subscripts relate to the composition parameter x. The ratio p does not depend on the Sternheimer factor and replaces the corresponding ratio of the s values.

The full lines in figure 6 show the calculated dependences of p on the $La_{2-x}Sr_xCuO_4$ composition for four possible versions of the spatial distribution of holes resulting from the substitution of Sr^{2+} for La^{3+}, when the holes reside at the copper sites, at the oxygen site O(1) lying in the La–O planes, at the oxygen sites O(2) lying in the Cu–O planes and at both types of oxygen sites simultaneously. The experimental values of P, also marked in figure 6, support the model implying the presence of holes at the O(2) sites. This conclusion is in good agreement with that made in our paper [6] on the basis of $^{67}Cu(^{67}Zn)$ Mössbauer data.

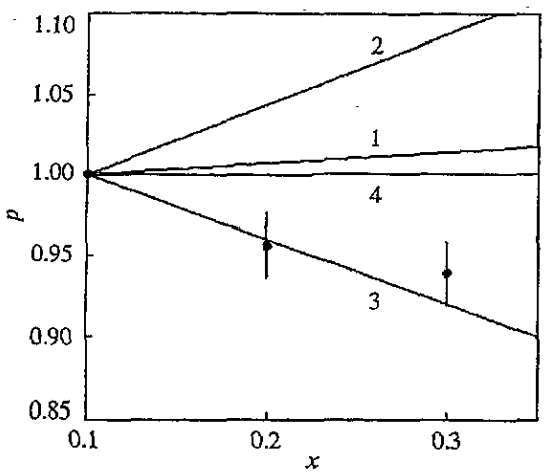

Figure 6. Dependence of the calculated ratio p (see the text) on the composition parameter x for the $La_{2-x}Sr_xCuO_4$ solid solutions with holes assumed to reside at the copper sites (line 1), at the O(1) sites (line 2), at the O(2) sites (line 3) and at the oxygen sites of both types (line 4). The circles show the experimental values of P.

4. Conclusions

$^{155}Eu(^{155}Gd)$ emission Mössbauer spectroscopy has been shown to be applicable for determining the parameters of the lattice EFG tensor at the REM sites of $RBa_2Cu_3O_7$ and $La_{2-x}Sr_xCuO_4$. The experimental EFG can be fitted by the calculated values if the holes are placed mainly at the chain and Cu–O plane oxygen sites of the $RBa_2Cu_3O_7$ and $La_{2-x}Sr_xCuO_4$ lattices, respectively.

Acknowledgment

This work was supported by the Russian Scientific Council on High-Temperature Superconductivity, project No 91139 'Resonance'.

References

[1] Adrian F J 1988 *Phys. Rev.* B **38** 2426
[2] Schwarz K, Ambrosch-Draxl C and Blaha P 1990 *Phys. Rev.* B **42** 2051
[3] Yu J, Freeman A J, Podloucky R, Herzig P and Weinberger P 1991 *Phys. Rev.* B **43** 532
[4] Seregin P P, Nasredinov F S, Masterov V F and Deribaeva G T 1990 *Phys. Status Solidi* a **159** K97
[5] Seregin N P, Nasredinov F S, Masterov V F and Daribaeva G T 1991 *Supercond. Sci. Technol.* **4** 283
[6] Seregin N P, Masterov V F, Nasredinov F S, Saidov Ch S and Seregin P P 1992 *Supercond. Sci. Technol.* **5** 675
[7] Masterov V F, Nasredinov F S, Seregin N P and Seregin P P 1992 *Superconductivity (KIAE)* **5** 1830
[8] Tarascon J M, McKinnen W R, Greene L H, Hull G W and Vogel E M 1987 *Phys. Rev.* B **36** 226
[9] LePage Y, Siegrist T, Sunshine S A, Schneemeyer L P, Murphy D W, Zahurak S M, Wazczak J W and McKinnen W R 1987 *Phys. Rev.* B **36** 3617
[10] Hanzawa K, Kawatsu E and Yashida K 1990 *J. Phys. Soc. Japan* **59** 3345
[11] Gupta R P and Sen S K 1973 *Phys. Rev.* A **8** 1169
[12] Yvon K and Francois M 1989 *Z. Phys.* B **76** 413
[13] Tarascon J M, Grene L H, McKinnen W R, Hull G W and Geballe T H 1987 *Science* **235** 1373